



Determining the factors affecting dynamic insertion of microneedles into skin

Sahan A. Ranamukhaarachchi¹ · Boris Stoeber^{1,2}

Published online: 19 November 2019
© Springer Science+Business Media, LLC, part of Springer Nature 2019

Abstract

Microneedles are extremely small and minimally-invasive intradermal drug delivery devices that require controlled, accurate, and repeatable insertions into human skin to perform their functions. Due to high variability and elasticity of human skin, dynamic insertion methods are being sought to ensure success in microneedle insertions into the skin passed the tough stratum corneum layer. Dynamic microneedle insertions have not been thoroughly studied to identify and assess the key parameters influencing the skin fracture to date. Here, we have utilized a previously validated artificial mechanical human skin model to identify and evaluate the factors affecting microneedle insertion. It was determined that a microneedle's velocity at impact against the skin played the most crucial role in successfully inserting microneedle devices of different geometrical features (i.e., tip area) and array size (i.e., number of projections). The findings presented herein will facilitate the development of automated microneedle insertion devices that will enable user-friendly and error-free applications of microneedle technologies for medicine delivery.

Keywords Microneedle · Dynamic insertion · Artificial skin · Skin crack propagation

1 Introduction

Microneedles (MNs) are projections with typically sub-millimeter heights that can overcome the stratum corneum (SC) layer of skin to provide mechanical pathways for intradermal drug delivery. MN-mediated drug delivery methods are minimally invasive, pain-free, and potentially self-administrable. Several studies have focused on characterizing MN insertions into skin to understand the factors affecting successful MN performance, in particular geometrical features of MNs (Davis et al., 2004; Yang & Zahn, 2004; Park et al., 2005; Khanna et al., 2010; Olatunji et al., 2013). However, due to the large variability in the mechanical properties of skin (Geerligs, 2006; Ranamukhaarachchi et al., 2016a), the results reported for MN insertion in different studies in the literature are difficult to compare and show inconsistencies (i.e., insertion force per MN ranged between 0.1–3.0 N (Davis et al., 2004; Yang & Zahn, 2004; Khanna et al., 2010)).

To overcome the variability of skin mechanics during the assessments of MN insertions, we developed and validated an artificial mechanical skin model to simulate the mechanical properties of human skin at low and high relative humidity conditions (Ranamukhaarachchi et al., 2016a). The artificial skin model consisted of three layers representing the stratum corneum, viable epidermis, and dermis; it is beneficial for studying MN-soft tissue interactions, and overcomes the limitations associated with biological skin, including the limited availability of fresh human skin samples, the difficulty of stretching skin to its *in vivo* configuration, and concerns regarding the safety of handling.

Several other artificial mechanical skin models have previously been fabricated from soft materials, such as polydimethylsiloxane, polyurethane, and hydrogels (Passot & Cabodevila, 2011; Koelmans et al., 2013; Larrañeta et al., 2014; Garland et al., 2012; Zhang et al., 2014). None of the suggested models have been validated against human skin, and only a few have been used to study the dynamic factors influencing MN insertions. For example, Koelmann, et al. used a double-layer artificial skin model to characterize the MN insertions into skin, and showed that increasing the velocity of impact increases the maximum force applied to the skin (Koelmans et al., 2013). However, the range of velocities assessed (up to 500 $\mu\text{m s}^{-1}$) were in the quasi-static regime of MN insertions. Due to the large range of energy that needs to be delivered to the skin through the MNs to ensure their

✉ Boris Stoeber
boris.stoeber@ubc.ca

¹ Department of Electrical and Computer Engineering, The University of British Columbia, Vancouver, BC V6T 1Z4, Canada

² Department of Mechanical Engineering, The University of British Columbia, Vancouver, BC V6T 1Z4, Canada

successful insertion passed the stratum corneum, as previously indicated by Chua et al. (Chua et al., 2013), a more thorough assessment of MN insertion dynamics is needed on a suitable and validated skin substrate.

The main objective of this study is to determine the key factors that contribute to the dynamics of MN insertion into a skin sample. Further, the influence of MN geometry on the insertion process into skin is assessed. The findings from this study will provide guidelines for successful MN insertion into human skin.

2 Materials and methods

2.1 Microneedles and skin model

Hollow metallic MNs were fabricated according to Mansoor, et al. using a metal electrodeposition process to obtain single MN devices (1-MN) with heights of $700 \pm 38 \mu\text{m}$, and outer tip diameters (OD) of $60 \pm 11 \mu\text{m}$, $100 \pm 14 \mu\text{m}$, and $120 \pm 15 \mu\text{m}$ (Mansoor et al., 2013). Further, hollow MN arrays consisting of 6 MNs (6-MN) of $700 \pm 38 \mu\text{m}$ height and $100 \pm 14 \mu\text{m}$ OD arranged in a hexagonal fashion and 19 MNs (19-MN) of $700 \pm 38 \mu\text{m}$ height and $100 \pm 14 \mu\text{m}$ OD arranged in a concentric layout (central MN surrounded by two rings of 6 and 12 MNs) were fabricated. The MNs were bonded to a plastic female Luer connector, which can be mounted to standard syringes with male Luer connectors.

An artificial mechanical skin model, previously designed and validated against human and porcine skin samples (Ranamukhaarachchi et al., 2016a), was employed to assess MN insertions. The artificial mechanical skin model, hereforth referred to as the skin model, was made of three layers mimicking the Young's moduli of the SC (85–110 MPa in an $18 \mu\text{m}$ layer), viable epidermis (9 kPa in a $200 \mu\text{m}$ layer), and the dermis (60 kPa in a 1 mm layer); the skin model provided a transparent substrate allowing skin cross-sectional visualization of MN insertions, without dimensional modifications, such as skin stretching. All layers were fabricated using several polydimethylsiloxane (PDMS) kits (Ranamukhaarachchi et al., 2016a).

2.2 Microneedle insertion setups

Quasi-static MN insertions were performed using a Q400 thermo-mechanoanalyzer (TMA; TA Instruments, DE, USA) as performed previously by Ranamukhaarachchi et al. (Ranamukhaarachchi et al., 2016b).

Dynamic MN insertions into the skin model were performed using a custom-built setup (Fig. 1). The spring-loaded MN insertion device included a Luer attachment for MN arrays (1-MN, 6-MN, or 19-MN). A locking mechanism (Fig. 1) with grooves allowed setting different

spring compression levels at the beginning of an experiment with compression levels ranging from 4 to 24 mm at 4 mm increments to set different levels of total dynamic energy for the insertion system. The insertion device also allowed changing the spring inside the main barrel to manipulate potential energy (E_p) and kinetic energy (E_k) of the system, respectively. The spring used in this study (spring constant, $k = 266 \text{ N m}^{-1}$) was purchased from WB Jones Springs Co. Inc. (KY, USA).

The artificial skin model was placed on a FS01 piezoresistive force sensor (Honeywell, NJ, USA). A light source illuminated the MN device and the skin model from the backside, providing a silhouette view of the MN relative to the skin model at all times, as shown in the bottom left corner of Fig. 1 (in the view finder of the high-speed camera). During each MN insertion experiment, force data was captured from the force sensor at a frequency of 100 kHz using a LabVIEW virtual instrument (National Instruments, TX, USA), along with high-speed image acquisition (208×200 -pixel image size) at 10,000 fps using a Phantom Miro 310 high-speed camera and the Phantom Camera Control software (Vision Research, NJ, USA). The force data capture was triggered by the image acquisition, which provided synchronization of the data from the two sources.

2.3 Dynamic microneedle insertion procedure

Prior to MN insertion, the insertion device was aligned with the surface of the skin model to ensure that the resting position of the spring occurred where the MN was fully inserted into the skin and the MN base was barely in contact with the skin model. The spring was then compressed to a pre-defined level on the device between 4 mm to 20 mm (Fig. 2A), and released to actuate the MN onto the skin model to perform the insertion (Fig. 2B). Force data and high-speed images were captured during each event.

2.4 Data processing and analysis

The force data recorded was used as-is during the analysis, while the captured images were further processed using Matlab (MathWorks, MA, USA), and used to determine the MN displacement as a function of time. Each image, captured originally in grayscale, was converted to a binary image in its full size based on a threshold of 0.25, which was determined based on the sensitivity of image artifacts to the binary threshold. All pixels in the grayscale image with luminance greater than the 0.25 threshold were replaced with 1 (white), while all other pixels were replaced with 0 (black). As the MN moved towards the skin frame-by-frame, the total number of white pixels reduced, allowing direct calculation of pixel displacement. The displacement in pixels was converted to millimeters using a calibration measurement. Since force data was

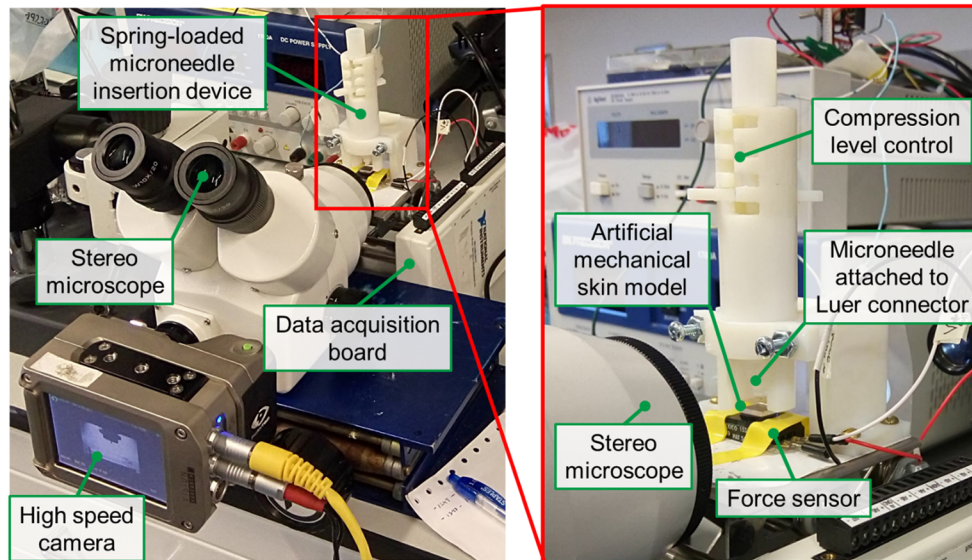


Fig. 1 Microneedle insertion setup includes a high-speed camera connected to a stereo microscope for image acquisition; a spring-loaded device for MN insertion; an artificial mechanical skin model on a force sensor that is connected to a data acquisition board to acquire and save

force data during MN insertion. The spring-loaded MN insertion device consists of multiple levels of spring compression providing control for energy introduced to the MN insertion. The MN-Luer device is attached to the spring-loaded insertion device

captured at a 10-fold higher frequency than the image acquisition, the displacement data was interpolated to match the force data using the Piecewise Cubic Hermite Interpolating Polynomial (PCHIP) function on Matlab. The velocity was calculated from the difference in displacement as a function of time.

2.5 Microneedle insertion experiments

2.5.1 Effect of velocity and energy on microneedle insertion

Several MN insertion experiments were conducted per the factorial design (Table 1). The 120 μm OD 1-MN device

was predominantly used to identify the key factors affecting MN insertions. Using the energy balance equation, the initial energy of the system (E_o) was calculated from the spring constant k and spring compression (x) distance:

$$E_o = \frac{1}{2} kx^2 \tag{1}$$

The expected velocity at impact (v_{imp}) was calculated from the kinetic energy at impact ($E_{k,imp}$) and moving mass (m):

$$E_{k,imp} = \frac{1}{2} mv_{imp}^2 \tag{2}$$

$$v_{imp} = \sqrt{\frac{2E_{k,imp}}{m}} \tag{3}$$

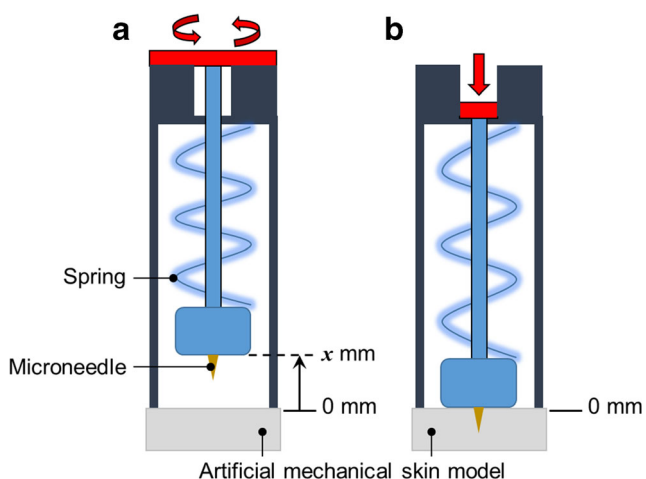


Fig. 2 Dynamic microneedle insertion steps. (A) The spring inside the insertion device is compressed to a pre-defined level (x) to input dynamic energy into the system and locked in position by a rotation mechanism. (B) The spring is released by rotation causing microneedle actuation on to the artificial mechanical skin model

2.5.2 Effect of momentum on microneedle insertion

The impact of the momentum on the force and energy required for successful MN insertion was assessed at constant total dynamic energy ($E_o = 1.2$ mJ), using the design of experiment in Table 2.

2.5.3 Effect of microneedle tip outer diameter on insertion

The impact of MN tip OD on insertion dynamics was assessed using 1-MN devices with 3 different tip ODs: 60 μm, 100 μm, and 120 μm. Each 1-MN device was inserted into the skin model using the quasi-static insertion test and the spring-

Table 1 Design of experiment to assess the impact of MN tip outer diameter on the insertion of a single microneedle with a 60, 100, and 120 μm tip OD ($m = 6$ g)

Microneedle tip OD (μm)	Insertion	Spring Compression, x (mm)	Dynamic energy of the system, E_o (mJ)	Expected velocity at impact, v_{imp} ($m\ s^{-1}$)	Trials per device (n)
60, 100, 120	Quasi-static	N/A	0	0	4
	Dynamic ($k = 266\ N\ m^{-1}$)	12	19.2	2.5	4
		20	53.2	4.2	4

loaded insertion device ($k = 266\ N\ m^{-1}$) at 12 mm and 20 mm spring compression levels, per Table 1.

2.5.4 Effect of the microneedle array size on the insertion

The effect of the number of MNs on the MN insertion dynamics was assessed using 1-MN, 6-MN and 19-MN devices. Each device was inserted into the skin model using the spring-loaded insertion device ($k = 266\ N\ m^{-1}$) at 12 mm and 20 mm spring compression levels, per Table 3. The single MN was also assessed using quasi-static insertion tests.

3 Results and discussion

3.1 Microneedle insertion profile

The force versus displacement curves were generated for each MN insertion until maximum force and displacement values were reached. The maximum force (ranged between ~8–17 N) recorded for each insertion resulted from the maximum displacement (~0.7 mm) of the MN into the skin, which corresponded to the height of the MN. An example of a MN insertion force versus displacement curve is provided in Fig. 3. Since the force sensor was located directly under the skin model sample, the first response from the force sensor only appeared at the initial point of impact of the MN on the skin model. As observed previously (Ranamukhaarachchi et al., 2016a) the force drops slightly as the needle breaks the SC. The data acquisition rate during dynamic insertions was not sufficiently high to measure this drop in force due to the high

velocity of the needle, and the force-displacement graph only showed a temporary change in slope. During quasi-static insertions, the drop in force due to the rupture of the SC is more prominent, as shown previously (Ranamukhaarachchi et al., 2016a).

From each MN insertion experiment, the following main independent variable defined was E_o , tip OD, and number of MNs in an array. The velocity at impact v_{imp} , the velocity at insertion v_{ins} , the momentum at impact $p_{imp} = m \cdot v_{imp}$ with the moving mass m , the momentum at insertion $p_{ins} = m \cdot v_{ins}$, the kinetic energy at impact $E_{k,imp}$ and the kinetic energy at insertion $E_{k,ins}$ were determined as covariates or predictors. From each MN insertion, the main dependent variables were the force of insertion F_{ins} , the energy required for insertion E_{ins} corresponding to the area under the force-displacement curve until the point of insertion, and the displacement at insertion D_{ins} , as previously described by Ranamukhaarachchi et al. (Ranamukhaarachchi et al., 2016b).

3.2 Factors affecting the dynamic insertion of a single microneedle

MN insertions were conducted using a single MN consisting of a 120 μm tip OD to determine if the process of rupturing the SC was a dynamic process. The impact of E_o and v_{imp} on F_{ins} and E_{ins} were evaluated. A decrease in the F_{ins} was observed as a function of v_{imp} , p_{imp} , and $E_{k,imp}$, which were manipulated by changing the E_o of the spring-loaded applicator. The mean percent difference between the estimated v_{imp} and measured v_{imp} across 84 measurements was calculated to be 1.1% ± 0.25%, according to:

$$\%Difference\ in\ v_{imp} = \left(\frac{estimated\ v_{imp} - measured\ v_{imp}}{estimated\ v_{imp}} \right) \times 100 \tag{4}$$

The F_{ins} decreased from 0.88 N to 0.37 N as v_{imp} increased from 0 to 4.2 $m\ s^{-1}$. The main variable in p_{imp} and $E_{k,imp}$ was v_{imp} , since the mass of the moving object was kept constant at 6 g in the design of experiment in Table 1. Therefore, v_{imp} of the MN on the skin model was identified as the driving factor

Table 2 Design of experiment to assess the impact of momentum on the insertion of a single microneedle with a 100 μm tip OD ($k = 266\ N\ m^{-1}$; $x = 4$ mm)

Dynamic energy of the system, E_o (mJ)	Moving mass, m (g)	Expected velocity at impact, v_{imp} ($m\ s^{-1}$)	Expected momentum at impact, p_{imp} ($kg\ m\ s^{-1}$)	Trials per device (n)
1.2	6	0.64	0.004	4
	21	0.34	0.007	4
	36	0.26	0.009	4

Table 3 Design of experiment to assess the impact of array size on MN insertion with single (1-MN), six (6-MN), and nineteen (19-MN) microneedle arrays consisting of projections with 100 μm tip OD ($k = 266 \text{ N m}^{-1}$)

Microneedle array size	Spring Compression, x (mm)	Dynamic energy of the system, E_o (mJ)	Expected velocity at impact, v_{imp} (m s^{-1})	Trials per device (n)
1, 6, 19	12	19.2	2.5	4
	20	53.2	4.2	4

influencing the F_{ins} (Fig. 4). This decrease in the F_{ins} as v_{imp} increased confirmed the dynamic nature of the MN insertion, which agreed with the observations by Heverly et al. (2005), who showed that F_{ins} of hypodermic needles into tissue also decreased with increasing v_{imp} up to a critical value. Heaverly et al. further showed that above the critical v_{imp} , the F_{ins} became independent of the v_{imp} (Heverly et al., 2005). Similarly to F_{ins} , the E_{ins} also decreased from 0.14 mJ to 0.04 mJ as v_{imp} increased from 0 to 4.2 m s^{-1} (Fig. 4). The impact of E_o and v_{imp} on F_{ins} and E_{ins} was also confirmed in single MNs with 60 μm and 100 μm tip OD (data not shown).

A possible reason for decreasing F_{ins} and E_{ins} as a function of v_{imp} was the development of a critical strain concentration in the SC of the skin model around the MN tip earlier to cause rupture during dynamic insertion, compared to quasi-static insertion. During quasi-static insertion of a MN, the stress was distributed across a larger region of the skin (up to a radius > 1.5 mm from the MN tip), and the displacement of the MN into the skin to reach the critical strain to cause SC failure was significantly higher. However, since skin is a viscoelastic material whose mechanical responses are strain-rate dependent, the findings presented in Fig. 4 were contradictory to the theory of viscoelasticity – at high v_{imp} , a higher strain-rate of the skin would have yielded a larger F_{ins} and E_{ins} . Therefore, along with reaching the ultimate tensile strength (UTS) of the skin faster, it was observed visually through the high-speed image acquisition of the insertion process that

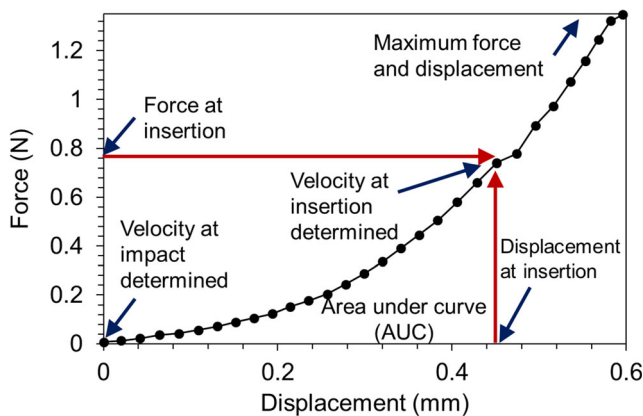


Fig. 3 Microneedle insertion force versus displacement profile generated from an experiment using a spring-loaded insertion device ($k = 152 \text{ N m}^{-1}$, $x = 4 \text{ mm}$, $E_o = 1.2 \text{ mJ}$, and estimated $v_{imp} = 0.6 \text{ m s}^{-1}$) collected from the high-speed camera (at 10 kfps) and the FS01 force sensor (at 100 kHz)

increasing v_{imp} would lead to changing the mode of fracture of the SC from mode-II fracture (typical for blunt-tipped structures and observed during quasi-static insertions) to mode-I fracture (typical for sharp-tipped structures). Since the fracture toughness of skin to mode-I fracture is significantly lower than mode-II fracture, a significant decrease in the F_{ins} and E_{ins} was observed during dynamic insertions.

3.3 Influence of momentum

The influence of p_{imp} on MN insertion was assessed by using a constant E_o at 1.2 mJ, and increasing the mass m from 6 g to 36 g to reduce of v_{imp} from 0.64 m s^{-1} to 0.26 m s^{-1} , respectively. This resulted in a p_{imp} range from 0.004–0.009 kg m s^{-1} . During this increase in p_{imp} , F_{ins} increased from 0.49 N to 0.74 N ($P = 0.006$) and E_{ins} increased from 0.07 mJ to 0.09 mJ ($P = 0.45$), but no significant influence of p_{imp} on the MN insertion was observed (Fig. 5). This suggested that MN insertions were more influenced by changing E_o of the system than by changing the momentum of the moving MN. Further investigations into the role of p_{imp} at higher E_o will be helpful to confirm the differences in the effects between v_{imp} and p_{imp} on MN insertion.

3.4 Influence of microneedle geometry

The effect of MN tip area on the F_{ins} and E_{ins} was assessed using three MN tip areas: $2.83 \times 10^{-9} \text{ m}^2$ (60 μm tip OD),

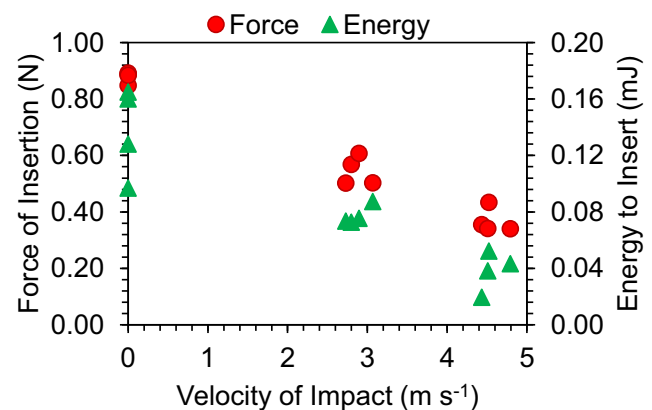


Figure 4 Factors influencing the insertion of a single microneedle into skin. Force and energy required to insert a single microneedle of outer tip diameters of 120 μm ($n = 12$), into the artificial skin model, as a function of the microneedle’s velocity at impact against the skin

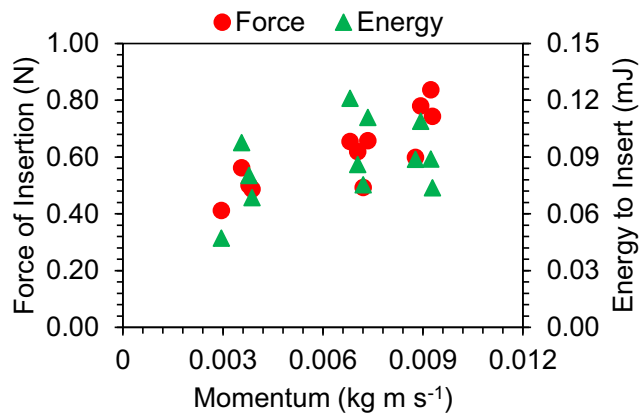


Fig. 5 Impact of momentum on the insertion of a single microneedle into skin. Force and energy required to insert a single microneedle of 100 μm outer tip diameter into the artificial skin model were determined ($n = 12$) at a constant total dynamic energy of 1.2 mJ. The momentum was altered by changing the moving mass m of the microneedle

$7.85 \times 10^{-9} \text{ m}^2$ (100 μm tip OD), and $1.13 \times 10^{-8} \text{ m}^2$ (120 μm tip OD). Each MN tip area was tested at three levels of total dynamic energy ($E_o = 0 \text{ mJ}$, 20 mJ, and 53 mJ; $n = 4$ per test condition) using a 3×3 factorial

design. The mean F_{ins} and E_{ins} from the MN insertions are provided in Table 4, which shows a significant increase in the F_{ins} and E_{ins} as the MN tip area increased ($P < 0.001$). Due to the increased area of the MN tip acting on the skin, a larger force needed to be applied to the skin to rupture through the SC. Increasing the E_o , which also increased the v_{imp} , decreased the F_{ins} and E_{ins} significantly ($P < 0.001$) for all tip areas (Fig. 6A and B). For example, during quasi-static insertion (where the total dynamic energy, $E_o = 0 \text{ mJ}$), increasing the tip area from $2.89 \times 10^{-9} \text{ m}^2$ to $1.13 \times 10^{-8} \text{ m}^2$ led to a significant increase in F_{ins} from 0.23 N to 0.88 N, respectively; however, dynamic insertions ($E_o = 53 \text{ mJ}$) caused a relatively reduced effect on the F_{ins} from 0.11 N to 0.37 N, respectively. Since the energy required per unit area of the MN tip to cause a crack was determined by the slope of the linear best fit in Fig. 6B, it provided an indirect indication of the fracture toughness of skin; the slope in Fig. 6B decreased from 10.1 J m^{-2} to 2.8 J m^{-2} as E_o increased from 0 to 53 mJ. This suggested that all MNs tested could rupture the SC at lower F_{ins} and E_{ins} as the dynamic energy introduced to the system increased, thereby reducing the deformation of the

Table 4 Effect of energy of the system (E_o) and the microneedle tip area on the force and energy required to insert a single microneedle into skin. The least significant difference (LSD, $P = 0.05$) is provided at a

95% confidence interval. Mean differences greater than the LSD indicate significantly different means between respective groups

Force of insertion, F_{ins} (N)						
Total dynamic energy, E_o (mJ)	Microneedle tip area (m^2)		7.85×10^{-9}		1.13×10^{-8}	
	Mean	SD	Mean	SD	Mean	SD
0	0.230	0.089	0.655	0.064	0.878	0.018
20	0.182	0.045	0.375	0.036	0.545	0.054
53	0.112	0.025	0.117	0.041	0.367	0.043
LSD ($P = 0.05$)	0.730					
MSE	0.003					
Error df	27					
N	4 each					
CV%	13.07					
Energy to insert, E_{ins} (mJ)						
Total dynamic energy, E_o (mJ)	Microneedle tip area (m^2)		7.85×10^{-9}		1.13×10^{-8}	
	Mean	SD	Mean	SD	Mean	SD
0	0.036	0.016	0.043	0.013	0.138	0.032
20	0.018	0.011	0.046	0.032	0.077	0.007
53	0.011	0.004	0.010	0.007	0.038	0.014
LSD ($P = 0.05$)	0.026					
MSE	0.000					
Error df	18					
n	4 each					
CV%	38.57					

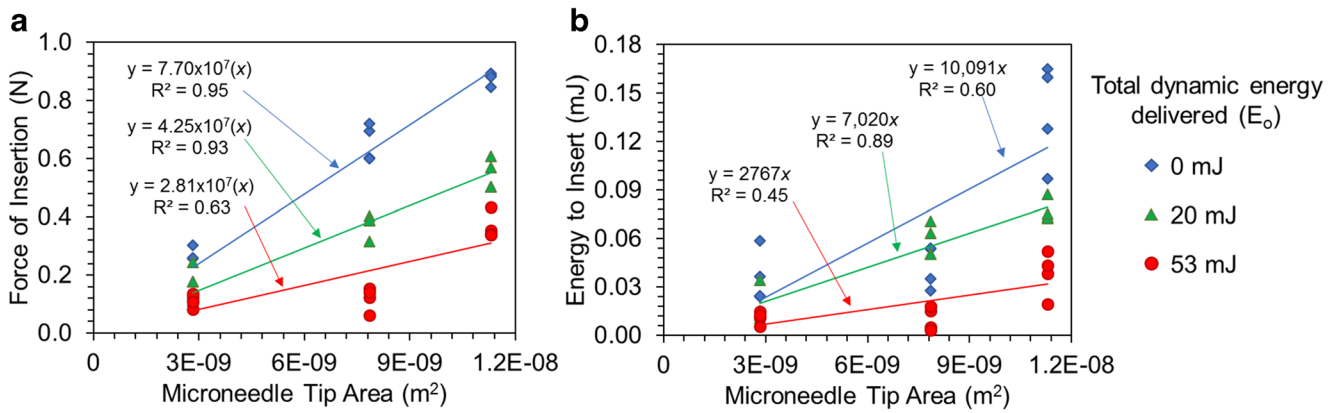


Fig. 6 Impact of microneedle tip area on skin insertion. (A) Force and (E) energy required to insert a single microneedle as a function of the microneedle tip area at three levels of total dynamic energy delivered ($E_o = 0, 20,$ and 53 mJ)

skin prior to rupture. This finding has a significant implication to the development of MN insertion protocols, since the introduction of E_o to the MN system will allow drastic reduction in the effort required to penetrate the SC of the skin for repeatable insertions for all MN tip areas.

3.5 Dynamic insertion of microneedle arrays

The effect of the number of MN projections in an array, with projections separated by 1 mm distance, on insertion dynamics (i.e., F_{ins} and E_{ins}) was assessed using three MN array configurations: 1-MN, 6-MN, and 19-MN (Fig. 7A). MN array insertions were assessed at $E_o = 20$ mJ and 53 mJ, using a 3×2 factorial design. Table 5 presents the mean F_{ins} and E_{ins} values recorded during the MN insertion tests.

For each MN configuration, increasing E_o from 20 mJ to 53 mJ led to a significant reduction in F_{ins} and E_{ins} ($P < 0.001$), as discussed earlier for single MN insertions. As the number of MNs increased from 1 to 19, the mean F_{ins} increased linearly from 0.38 N to 11.29 N at $E_o = 20$ mJ and 0.12 N to 7.83 N at $E_o = 53$ mJ. Similarly, the mean E_{ins} increased linearly from 0.05 mJ to 2.32 mJ at $E_o = 20$ mJ and 0.01 mJ to 6.69 mJ at $E_o = 53$ mJ. This can be further visualized in Fig. 7B and C, and suggested that MNs in arrays separated by 1 mm acted independently of each other and that the radius of deformation surrounding each MN was less than 0.5 mm during dynamic conditions. As a result, a significant interaction between the MN array size and the E_o was observed in Table 5 for F_{ins} and E_{ins} , demonstrating their synergistic effect on successful rupturing of the SC layer.

a Microneedle array size

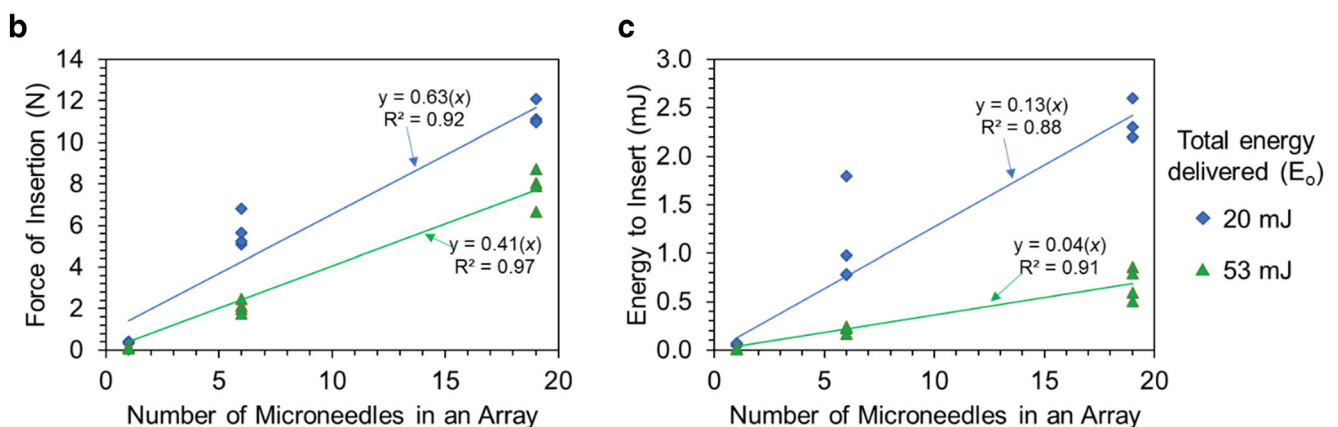


Fig. 7 Impact of the number of microneedles in an array on skin insertion. (A) Microneedle array sizes used in the study consisted of 1 (1-MN), 6 (6-MN), and 19 (19-MN) projections with 100 μ m tip outer

diameter. (B) Force and (C) energy required to insert microneedle arrays as a function of the number of microneedle projections in an array, measured at two levels of total dynamic energy delivered (20 and 53 mJ)

Table 5 Effect of energy of the system (E_o) and the number of microneedles in an array on the force and energy required to insert a single microneedle into skin. The least significant difference (LSD, $P=0.05$) is provided at a 95% confidence interval. Mean differences greater than the LSD indicate significantly different means between respective groups

Force of insertion, F_{ins} (N)						
Energy, E_o (mJ)	Number of microneedles					
	1		6		19	
	Mean	SD	Mean	SD	Mean	SD
20	0.375	0.037	5.703	0.789	11.293	0.529
53	0.118	0.040	2.080	0.293	7.833	0.855
LSD ($P=0.05$)	0.796					
MSE	0.287					
Error df	18					
n	4 each					

Energy to insert, E_{ins} (mJ)						
Energy, E_o (mJ)	Number of microneedles					
	1		6		19	
	Mean	SD	Mean	SD	Mean	SD
20	0.046	0.032	1.080	0.485	2.320	0.189
53	0.010	0.007	0.215	0.033	0.688	0.167
LSD ($P=0.05$)	0.332					
MSE	5.0×10^{-5}					
Error df	18					
n	4 each					

In contrast, skin deformation surrounding a MN during quasi-static insertion tests provided visual confirmation that the radius of the deformed area increased up to 1.5 mm with MN displacement (up to 700 μm). It is therefore probable that MNs separated by only 1 mm would be acting independently during dynamic insertions, but not during quasi-static MN insertion. It is also possible that the correlation between the F_{ins} or E_{ins} and the number of MNs will deviate from linearity beyond a certain threshold number of projections per array during quasi-static insertions. Therefore, developing MN insertion protocols using dynamic conditions appeared to be more favorable in ensuring successful insertion of MN arrays, compared to quasi-static insertions. Further investigation into the nature of MN interactions in an array during MN insertion will be beneficial.

4 Conclusions

Using an artificial skin model that was previously validated for mechanical similarity to human skin, the dynamics of MN insertions have been characterized. Using extremely high rates of data acquisition, this study provided insight on key factors

that significantly influenced successful MN insertions passed the skin's SC layer, including E_o , v_{imp} , MN tip area, and the number of projections. By increasing E_o , the v_{imp} of the MN device increased, which helped to significantly decrease the force and energy required to insert the MN device into the skin. Reducing the tip area of the MN led to the reduction in force and energy to insert the MNs. Increasing the number of microneedles in an array led to a linear increase with the number of needles in force and energy to insert the MNs during dynamic insertions. The understanding of these mechanical relationships will facilitate the development MN devices and insertion protocols to increase the success of intradermal drug delivery and biosensing approaches.

Acknowledgements The authors also thank the Vanier Canada Graduate Scholarship program, the Canadian Institute for Health Research, and the Natural Sciences and Engineering Research Council of Canada for financial contributions towards this research. This research was undertaken, in part, thanks to funding from the Canada Research Chairs program. The authors also thank Dr. Hasitha Jayathilake for his guidance on image processing for this study.

References

- S.P. Davis, B.J. Landis, Z.H. Adams, et al., *J. Biomech.* **37**, 1155 (2004)
- M. Yang, J.D. Zahn, *Biomed. Microdevices* **6**, 177 (2004)
- J.-H. Park, M.G. Allen, M.R. Prausnitz, *J. Control. Release* **104**, 51 (2005)
- P. Khanna, K. Luongo, J.A. Strom, et al., *J. Micromech. Microeng.* **20**, 045011 (2010)
- O. Olatunji, D.B. Das, M.J. Garland, et al., *J. Pharm. Sci.* **102**, 1209 (2013)
- M. Geerligs, Technical Note PR-TN 450 (2006)
- S.A. Ranamukhaarachchi, T. Schneider, S. Lehnert, et al., *Macromol. Mater. Eng.* **301**, 306 (2016a)
- A. Passot, G. Cabodevila, in *Mechanical properties of an artificial vascularized human skin*, (2011) (International Society for Optics and Photonics), p. 80680C
- W. Koelmans, G. Krishnamoorthy, A. Heskamp, et al., *Mech. Eng. Research* **3**, p51 (2013)
- E. Larrañeta, J. Moore, E.M. Vicente-Pérez, et al., *Int. J. Pharm.* **472**, 65 (2014)
- M.J. Garland, K. Migalska, T.-M. Tuan-Mahmood, et al., *Int. J. Pharm.* **434**, 80 (2012)
- D. Zhang, D.B. Das, C.D. Rielly, *J. Pharm. Sci.* **103**, 613 (2014)
- B. Chua, S.P. Desai, M.J. Tierney, et al., *Sens. Actuators A Phys.* **203**, 373 (2013)
- I. Mansoor, Y. Liu, U. Häfeli, et al., *J. Micromech. Microeng.* **23**, 085011 (2013)
- S. Ranamukhaarachchi, S. Lehnert, S. Ranamukhaarachchi, et al., *Sci. Rep.* **6** (2016b)
- M. Heverly, P. Dupont, J. Tiedman, in *Trajectory optimization for dynamic needle insertion*, 2005 (IEEE), p. 1646

Publisher's note Springer Nature remains neutral with regard to jurisdictional claims in published maps and institutional affiliations.